Development of Matrix Converter Interfaced Wind Energy Conversion System

[1]Bhavika Rathore, [2]Monika Vardia, [3]Bheru Das Vairagi
[1]Student M.Tech (Power Systems), [2]Associate Professor, [3]Assistant Professor
[1,2,3] Department of Electrical Engineering,
[1,2,3]Geetanjali Institute of Technology, Udaipur, India

Abstract : ***This paper presents the modelling and development of different components of the proposed matrix converter (MC) wind energy conversion system (WECS). The proposed system is developed using MATLAB/Simulink. In this work, a wind turbine emulator which drives the PMSG is used for laboratory tests. A space vector pulse width modulation (SVPWM) switching has been used to enhance dynamic performance under various balanced/unbalanced conditions. The main objectives of this work is to develop Space Vector PWM control for matrix converter interfaced Wind Energy Conversion System and to validate the proposed Wind Energy Conversion System and its control algorithms in simulation environment under various balanced /unbalanced conditions. It also investigates the performance of the hardware laboratory prototype of proposed wind generation system under various balanced /unbalanced conditions.***

Index Terms - Matrix Converter (MC); wind energy conversion system (WECS); space vector pulse width modulation (SVPWM).

I. INTRODUCTION

On the basis of the state-of-the-art in WECS research, this work aims to investigate the performance of Matrix Converter interfaced Wind Energy Conversion System for two reasons: first, matrix converter is an emerging technology with the potential of replacing AC/DC/AC converter, and second, no thorough experimental investigation of proposed WECS system has been made under abnormal conditions, e.g., load unbalance/ balance and varying wind conditions [1]. The main objectives of this work is to develop Space Vector PWM control for matrix converter interfaced WECS and to validate the proposed Wind Energy Conversion System and its control algorithms in simulation environment under various balanced /unbalanced conditions.

II. THE PROPOSED WIND ENERGY CONVERSION SYSTEM

Figure 1 shows the block diagram of the proposed unidirectional MC interfaced PMSG based wind energy conversion system [2]. As it can be seen in Fig.1, MC is used for interfacing with the laod/grid, and SVPWM control is effectively used to achieve low harmonic characteristics. It also performs power factor (pf) control at grid interface and satisfies the reactive power demand [3].

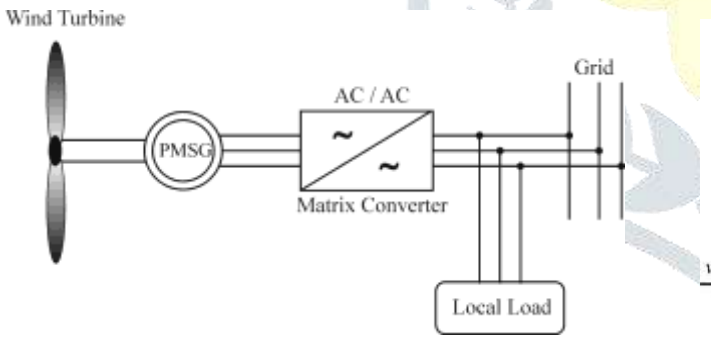

Fig. 1: Proposed Wind Energy Conversion System

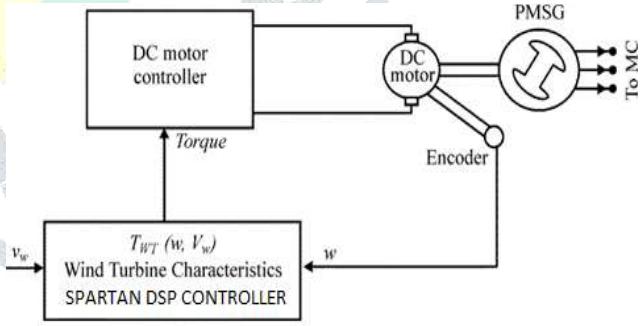

Fig. 2: Wind Emulator System

Wind Turbine Model

A wind turbine emulator which drives the PMSG is developed for laboratory tests. Figure 2 presents the structure of the wind emulator. The wind speed changes and load switching conditions are performed using the wind turbine emulator, which consists of chopper dc drive [4]. It obtains the wind speed values and, by using the turbine characteristics and dc motor speed, calculates the torque command of the wind turbine. In this way, it is able to reproduce the steady and dynamic behavior of a real wind turbine to the energy conversion system.

The aerodynamic torque (T_m) and power captured ($P_{0)}$ by a wind turbine is given by:

$$T_m = \frac{1}{2}\pi\rho C_p(\lambda) R_\omega^3 V_w^2 \quad (1)$$

$$P_0 = \frac{1}{2}\rho C_p A_r V_w^3 \quad (2)$$

where P_0 is the power in watt, ρ the air density in kg/m^3, C_p a dimensionless factor called power coefficient, A_r the turbine rotor area in m^2 ($A_r = \pi R_r^2$, where R_r is the rotor blade radius), and V_w wind speed in m/s.

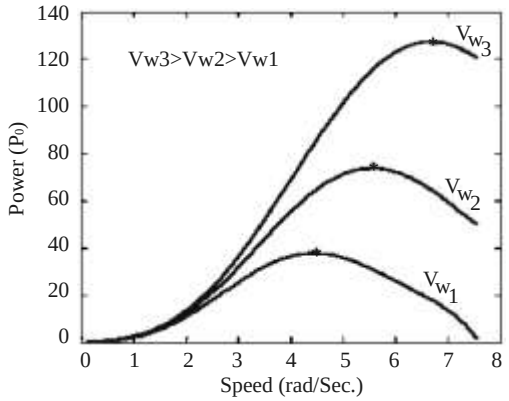

Fig. 3: Power-speed characteristics of a wind turbine for different wind velocities

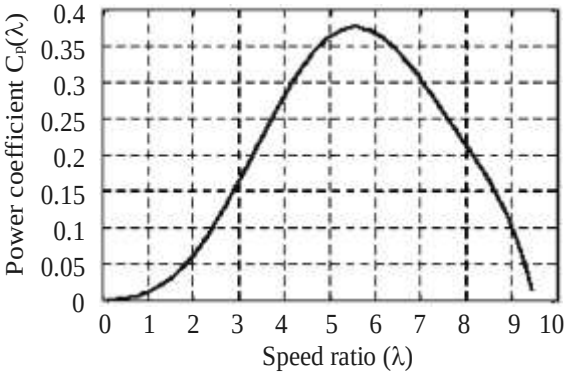

Fig. 4: C_P _ λ characteristics of wind turbine

Figure 3 illustrates the steady-state power-speed characteristics and the maximum power point attained at each wind speed (marked with star). The power coefficient is related to the tip speed ratio λ and rotor blade pitch angle θ, as shown in Fig.4.

Dynamic Model of Reversed Voltage-Boosted Matrix Converter

The schematic diagram of the unidirectional voltage-boosted matrix converter with twelve switches (clamping circuit is not shown here) is shown in Fig.5 (a). It consists of six switches with anti-parallel diodes are arranged as front end voltage source rectifier (VSR), whereas other six switches with series diodes as rear end current source inverter (CSI). It has its power flow from VSR to CSI terminals, which is the reverse direction of traditional matrix converter. This reversal is important with aspect to wind generation system as these require voltage boosting of its source with power flowing to grid or local loads [4].

At any instant, two switches each from upper and lower group of conducts. An active state is formed when two conducting switches are from different phase legs, whereas idle state is formed when conducting switches are from same phase legs. During active state, power is transferred to load, whereas during idle state circulating current flow within the MC due to shorting of fictitious dc voltage to zero. Space vector representation of CSI and VSR are shown in Fig.5 (b), where there are total three idle and six active states.

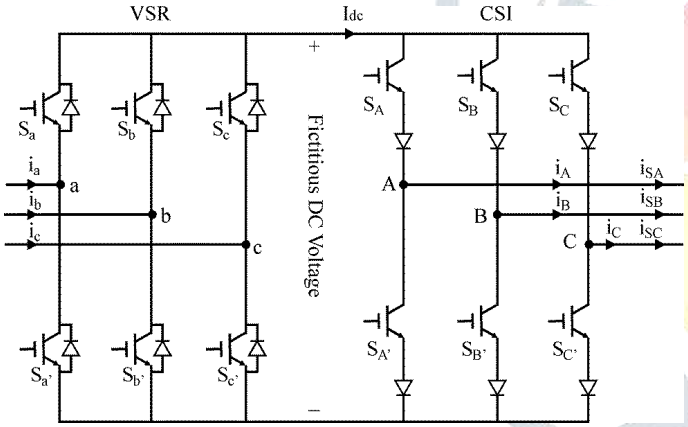

Fig. 5(a): Schematic diagram of the voltage boosted MC topology

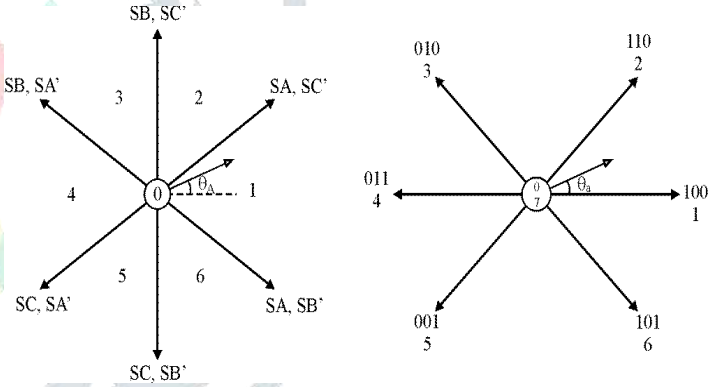

Fig. 5(b): Space vector representation for CSI and VSR of MC

Since input terminal a, b and c are connected to voltage sources, they must not be short-circuited through the MC switches. Similarly, as output terminals A, B and C are connected to current sources, they must not be open-circuited at any instant [5] & [6]. Based on these constraints, the switching function for each switch is:

$$S_{Kj} = \begin{cases} 1, & switch\ S_{Kj} \quad close \\ 0, & switch\ S_{Kj} \quad open \end{cases} \tag{3}$$

where,

K = {A, B, C}, j = {a, b, c},

and $S_{Ka} + S_{Kb} + S_{Kc} = 1,\ K = \{A, B, C\}$ (4)

The relationship between input and output instantaneous phase voltages are:

$$\begin{bmatrix} v_A \\ v_B \\ v_C \end{bmatrix} = \begin{bmatrix} S_{Aa} & S_{Ab} & S_{Ac} \\ S_{Ba} & S_{Bb} & S_{Bc} \\ S_{Ca} & S_{Cb} & S_{Cc} \end{bmatrix} \begin{bmatrix} v_a \\ v_b \\ v_c \end{bmatrix} \tag{5}$$

where v_A, v_B, v_C (v_a, v_b, v_c) are the output (input) voltages.

Based on (5), line-to-line voltages (phase currents) at the output (input) terminals are:

$$\begin{bmatrix} v_{AB} \\ v_{BC} \\ v_{CA} \end{bmatrix} = \begin{bmatrix} S_{Aa} - S_{Ba} & S_{Ab} - S_{Bb} & S_{Ac} - S_{Bc} \\ S_{Ba} - S_{Ca} & S_{Bb} - S_{Cb} & S_{Bc} - S_{Cc} \\ S_{Ca} - S_{Aa} & S_{Cb} - S_{Ab} & S_{Cc} - S_{Ac} \end{bmatrix} \begin{bmatrix} v_a \\ v_b \\ v_c \end{bmatrix} \quad (6)$$

$$\begin{bmatrix} i_a \\ i_b \\ i_c \end{bmatrix} = \begin{bmatrix} S_{Aa} & S_{Ba} & S_{Ca} \\ S_{Ba} & S_{Bb} & S_{Cb} \\ S_{Ac} & S_{Bc} & S_{Cc} \end{bmatrix} \begin{bmatrix} i_A \\ i_B \\ i_C \end{bmatrix} \quad (7)$$

where v_{AB}, v_{BC}, v_{CA} (i_A, i_B, i_C) are the output instantaneous voltages (currents), and i_a, i_b, i_c are the input instantaneous phase currents. The averaged equivalents corresponding to (6) and (7) are:

$$\begin{bmatrix} \tilde{v}_{AB} \\ \tilde{v}_{BC} \\ \tilde{v}_{CA} \end{bmatrix} = D \begin{bmatrix} v_a \\ v_b \\ v_c \end{bmatrix} \quad (8)$$

Where

$$D = \begin{bmatrix} d_{Aa} - d_{Ba} & d_{Ab} - d_{Bb} & d_{Ac} - d_{Bc} \\ d_{Ba} - d_{Ca} & d_{Bb} - d_{Cb} & d_{Bc} - d_{Cc} \\ d_{Ca} - d_{Aa} & d_{Cb} - d_{Ab} & d_{Cc} - d_{Ac} \end{bmatrix} \quad (9)$$

$$\begin{bmatrix} \tilde{i}_a \\ \tilde{i}_b \\ \tilde{i}_c \end{bmatrix} = \begin{bmatrix} d_{Aa} & d_{Ba} & d_{Ca} \\ d_{Ab} & d_{Bb} & d_{Cb} \\ d_{Ac} & d_{Bc} & d_{Cc} \end{bmatrix} \begin{bmatrix} i_A \\ i_B \\ i_C \end{bmatrix}$$

Transformation of three-phase variables from abc to dq0 coordinates is given by:

$$f_{dq0} = T(\theta) f_{abc} \quad (10)$$

Where

$f_{dq0} = [f_d\ f_q\ f_0]^T$, $f_{abc} = [f_a\ f_b\ f_c]^T$, and

$$T(\theta) = \frac{2}{3} \begin{bmatrix} \cos\theta & \cos(\theta - \frac{2\pi}{3}) & \cos(\theta + \frac{2\pi}{3}) \\ -\sin\theta & -\sin(\theta - \frac{2\pi}{3}) & -\sin(\theta + \frac{2\pi}{3}) \\ \frac{1}{2} & \frac{1}{2} & \frac{1}{2} \end{bmatrix} \quad (11)$$

Without the loss of generality, θ for the input dq0 frame is set to $\omega_i t + \phi_i$, where ϕ_i can assume an arbitrary value. Thus, the input phase voltages and the corresponding dq0 quantities are related by:

$$v_{dq0} = T(\omega_i t + \phi_i) v_{abc} \quad (12)$$

 for the output dqo frame is set to $\omega_o t$, where ω_o is the grid synchronous frequency. Thus, the output line-to-line voltages and the corresponding dqo quantities are related by:

$$v_{DQO} = \frac{1}{\sqrt{3}} T\left(\omega_o t + \frac{\pi}{6}\right) v_{ABC,\,II} \quad (13)$$

where vABC, II = [vAB vBC vCA]T. Substitute for vABC, II and vabc from (12) and (13), respectively, in (7), we deduce:

$$\sqrt{3}\, T^{-1}\left(\omega_o t + \frac{\pi}{6}\right) v_{dqo} = D T^{-1}(\omega_i t + \varphi_i) v_{dq0} \quad (14)$$

From (13),we deduce

$$v_{dqo} = \sqrt{3}\, T\left(\omega_o t + \frac{\pi}{6}\right) D T^{-1}(\omega_i t + \varphi_i) v_{dq0} = D_{dq0} v_{dq0} \quad (15)$$

where D_{dq0} is defined as

$$D_{dq0} = \sqrt{3}\, T\left(\omega_o t + \frac{\pi}{6}\right) D T^{-1}(\omega_i t + \varphi_i) \quad (16)$$

Since input/output circuits do not contain zero-sequence components, from (3.14), and (3.15) we deduce:

$V_{dq} = D_{dq} v_{dq}$ (17)

where, $v_{dq} = [v_D\ v_Q]^T$, $v_{dq} = [v_d\ v_q]^T$

$$D_{dq} = \frac{m}{\cos\phi_i} \begin{bmatrix} \cos\phi_o \cos(\phi_i + \varphi_i) & -\cos\phi_o \sin(\phi_i + \varphi_i) \\ -\sin\phi_o \cos(\phi_i + \varphi_i) & \sin\phi_o \sin(\phi_i + \varphi_i) \end{bmatrix} \quad (18)$$

Similarly, it can be deduce the current relationship between the input and output direct-and quadrature-axis quantities as

$$i_{dq} = D_{dq}^{T} i_{dq} \quad (19)$$

where $i_{dq} = [i_d\ i_q]^T$, and $i_{dq} = [i_d\ i_q]^T$

i_{dq} relates the input dq current/ voltage components with the output dq current/ voltage components, and we define it as the dq switching function matrix for the MC. Equations (17) and (19) provide a dynamic model of the SVM-switched MC for WECS system.

Modelling of PMSG

The voltage equations of the PMSG in synchronous d-q coordinates can be expressed as:

$$v_{ds} = R_s i_{ds} + L_s \frac{di_{ds}}{dt} - w_r L_d i_{qs} \quad (20)$$

$$v_{qs} = R_s i_{qs} + L_s \frac{di_{qs}}{dt} + w_r L_q i_{ds} + w_r \lambda_f \quad (21)$$

where v_{ds} and v_{qs} are the d-axis and q-axis stator voltages, i_{ds} and i_{qs} are the d-axis and q-axis stator currents, L_d and L_q are the d-axis and q-axis inductances, R_s and L_s are the stator resistance and inductance, λ_f and w_r are the magnetic flux and angular speed of generator, respectively[7].

Figure 6 shows the d-q equivalent circuits of the PMSG. Therefore, the electromagnetic torque T_e can be expressed as:

$$T_e = \frac{3}{4} p \lambda_f i_{qs} \quad (22)$$

where p is the number of poles.

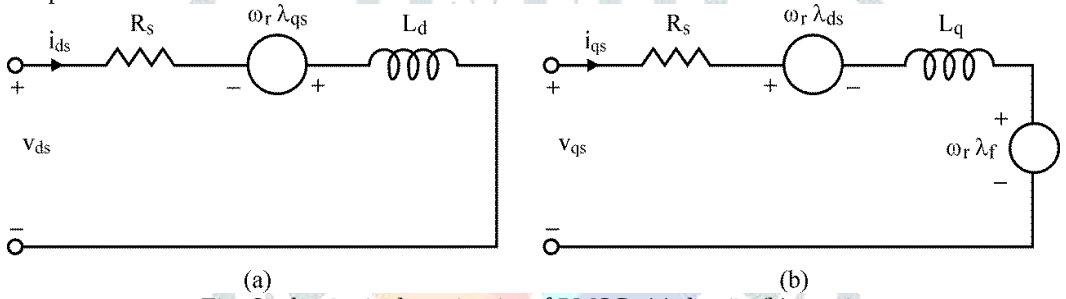

Fig. 6: d-q equivalent circuits of PMSG. (a) d-axis, (b) q-axis

III. Implementation of Proposed System using MATLAB/Simulink

Figure 7 presents the MATLAB/Simulink model of the matrix converter interfaced wind energy conversion system, which effectively uses the space vector modulation switching technique to have low harmonic characteristics with improved load voltage and current. Also, the Fig. 8 11 present the different simulink model for the space vector modulation based switching applied to the rectifying and inverting stage of the matrix converter used for the WECS.

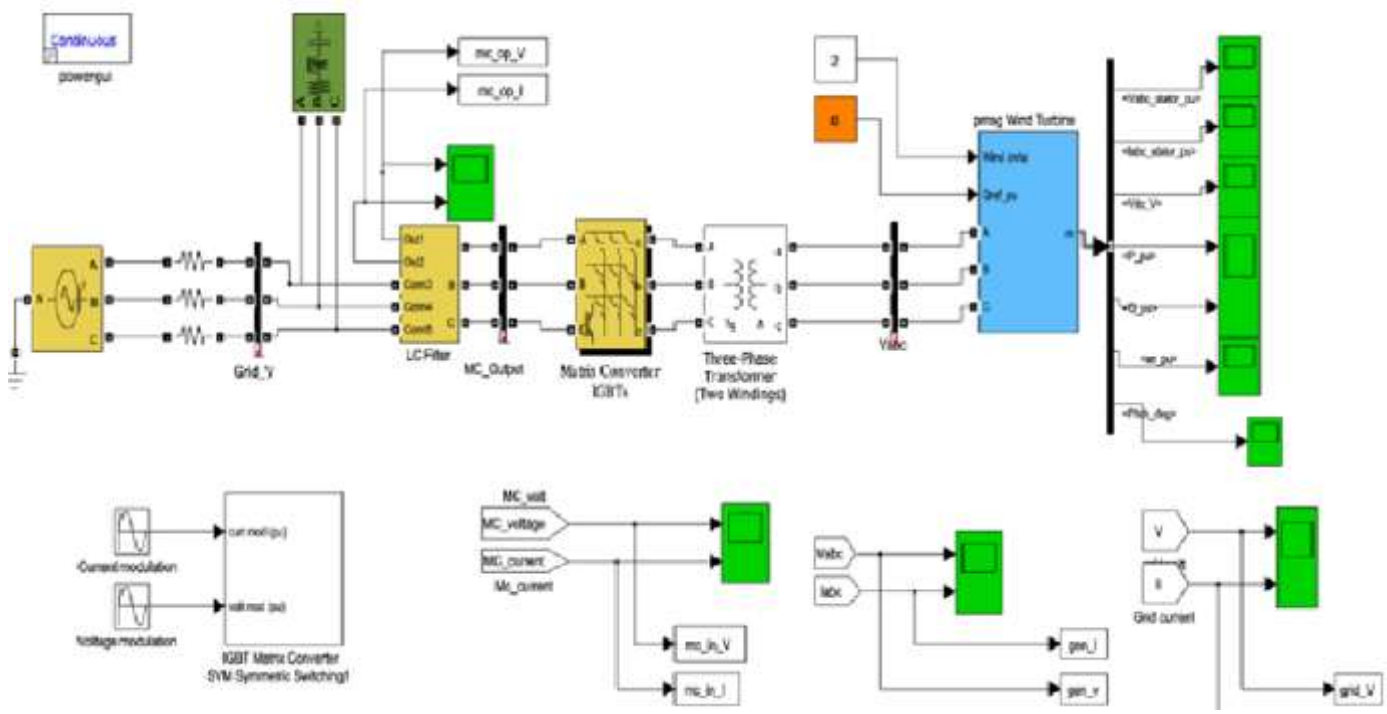

Fig. 7 : Simulink Model of space vector modulation switching based matrix converter applies to a wind energy conversion system

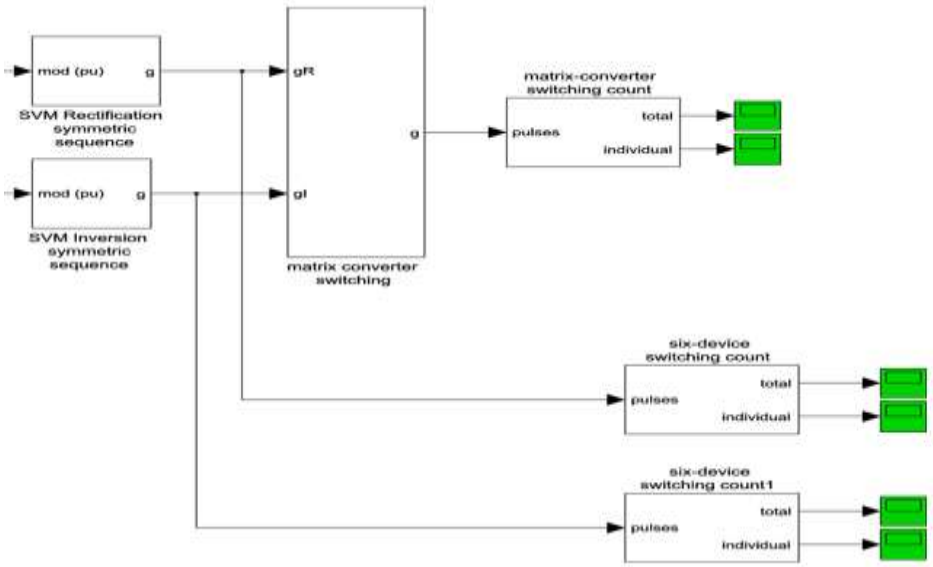

Fig. 8 : Simulink Model of the SVM switching based matrix converter applied to WECS

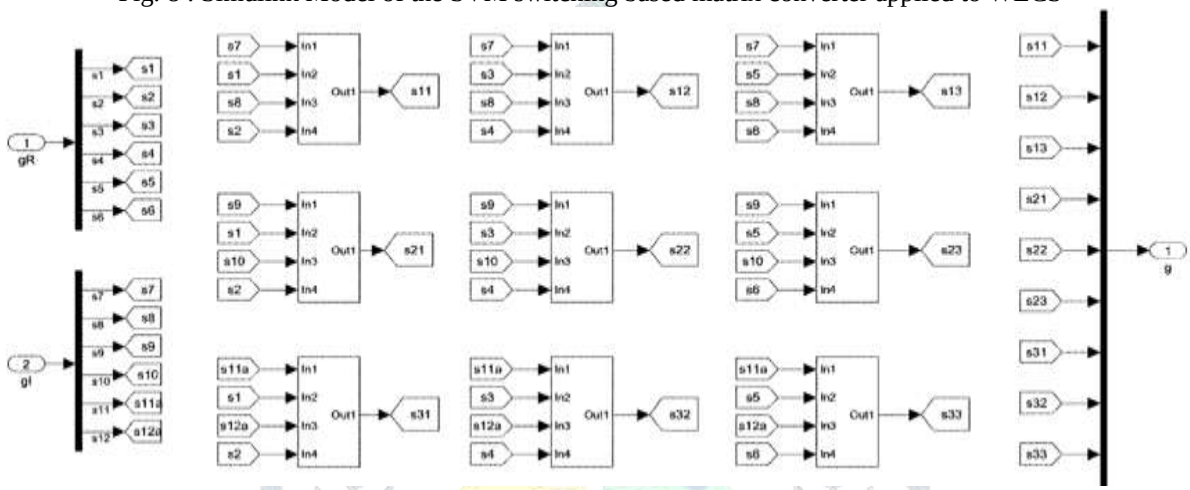

Fig. 9 : Simulink Model of Matrix converter switching

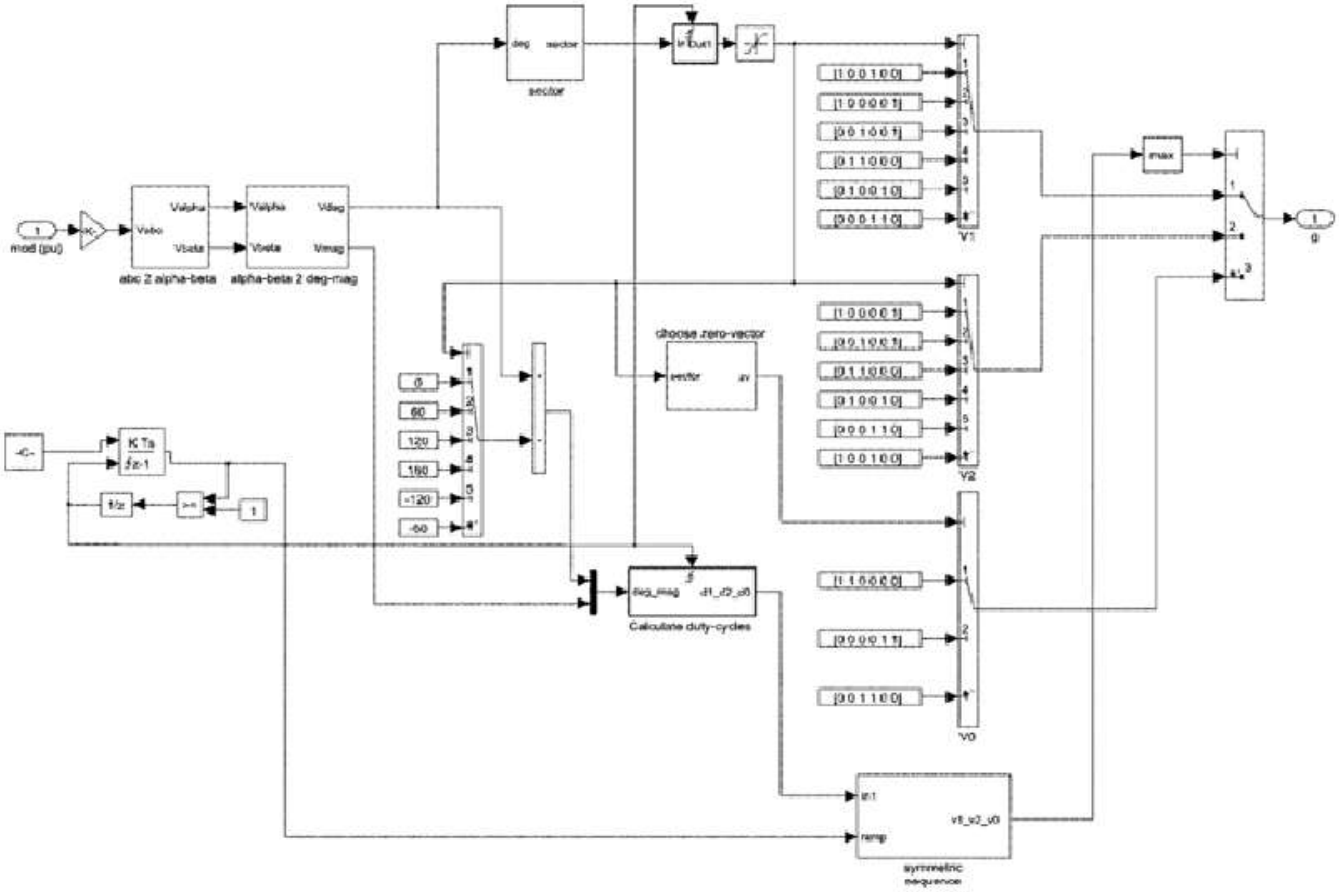

Fig. 10 : Simulink model of SVM rectification symmetric sequence

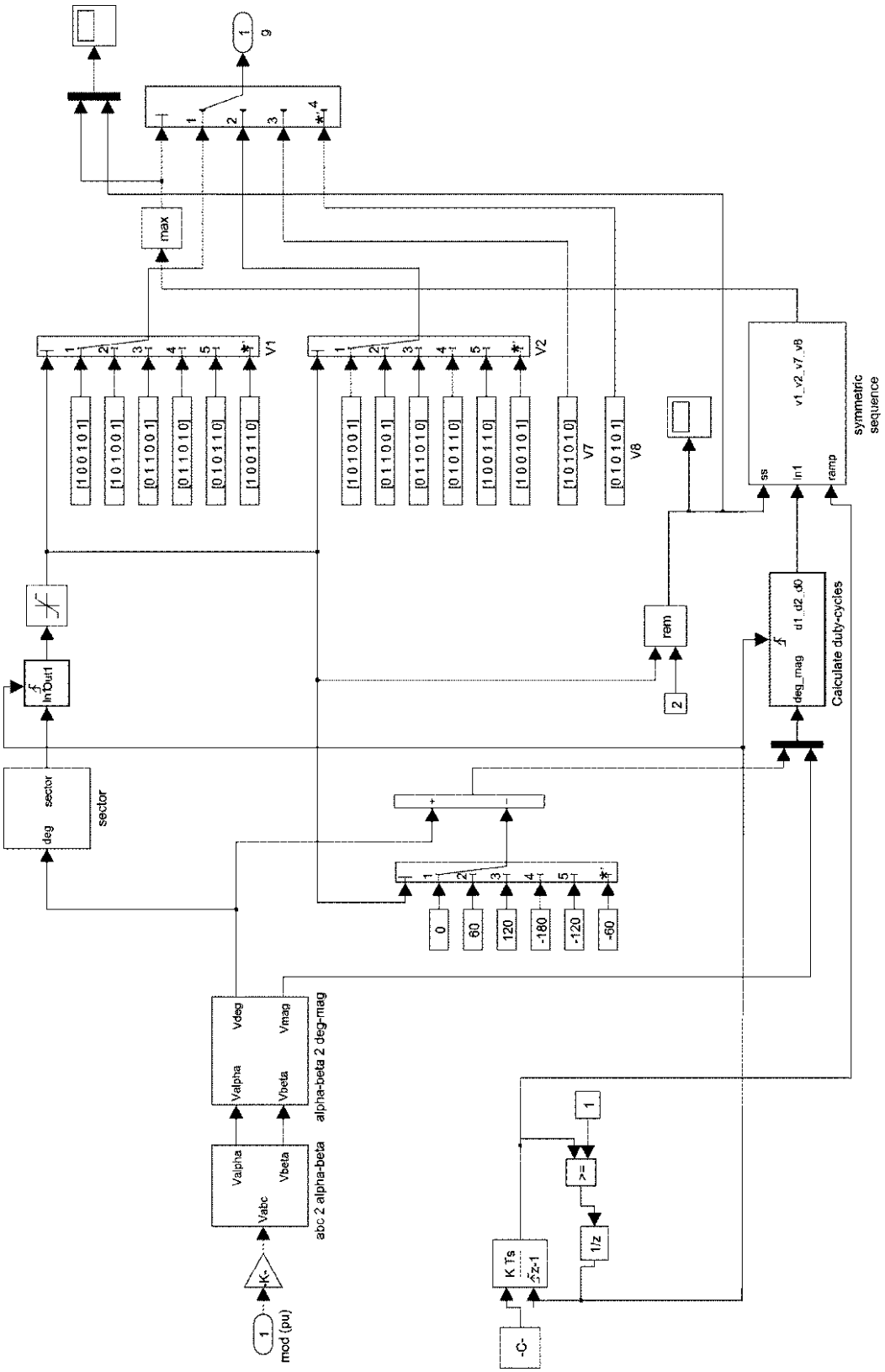

Fig. 11 : Simulink model of SVM inversion symmetric sequence.

IV. DETAILS OF LABORATORY PROTOTYPE OF WIND TURBINE EMULATOR

To study the effects of balanced/unbalanced input-output conditions on the wind power generation, a detailed laboratory test is carried out on 1.2 kW prototype of matrix converter interfaced wind energy conversion system using Spartan DSP controller environment[8]. Figure 12 presents the schematic of the test rig setup used for the experimental study. To verify the wind simulator operation, the speed of the shaft is changed by implementing a speed loop control. At different speeds, the input power to the matrix converter is measured. The measured power points are recorded, and the plot of the generator speed versus output power is generated as shown in Fig. 13.

Fig. 12: Schematic of the experimental setup of matrix converter interfaced PMSG for wind energy conversion system

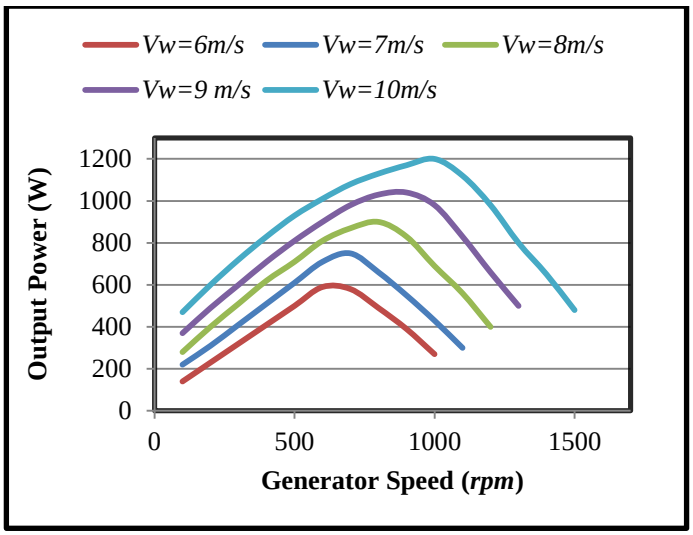

Fig. 13: Experimental plot of generator speed versus output power for different wind speeds

Space vector pulse width modulation based switching signals given to the switches of matrix converter and dc drive based wind turbine emulator are presented in Fig. 14. Three-phase variable resistive load, diode bridge rectifier-inverter fed induction motor and diode bridge rectifier fed dc motor is used as non-linear inductive ac/dc loads[9]-[10].

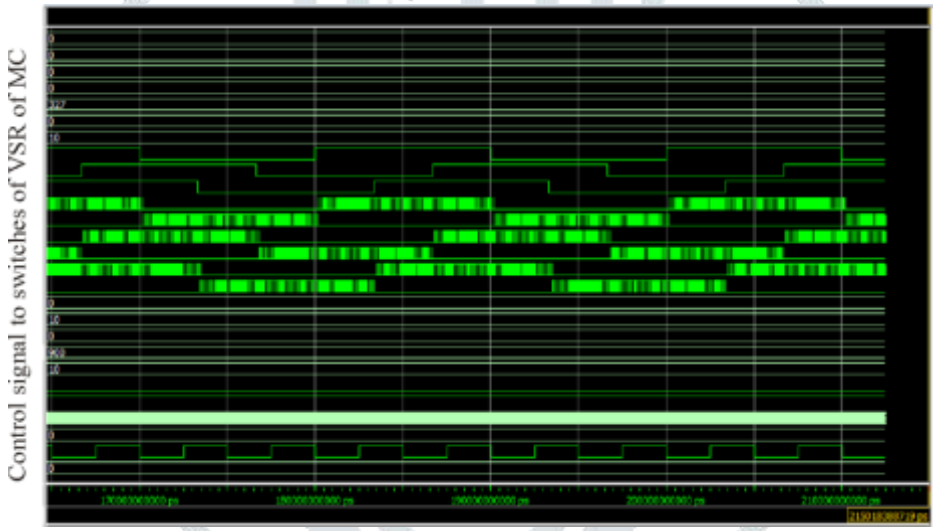

(a) Control signal to VSR of MC

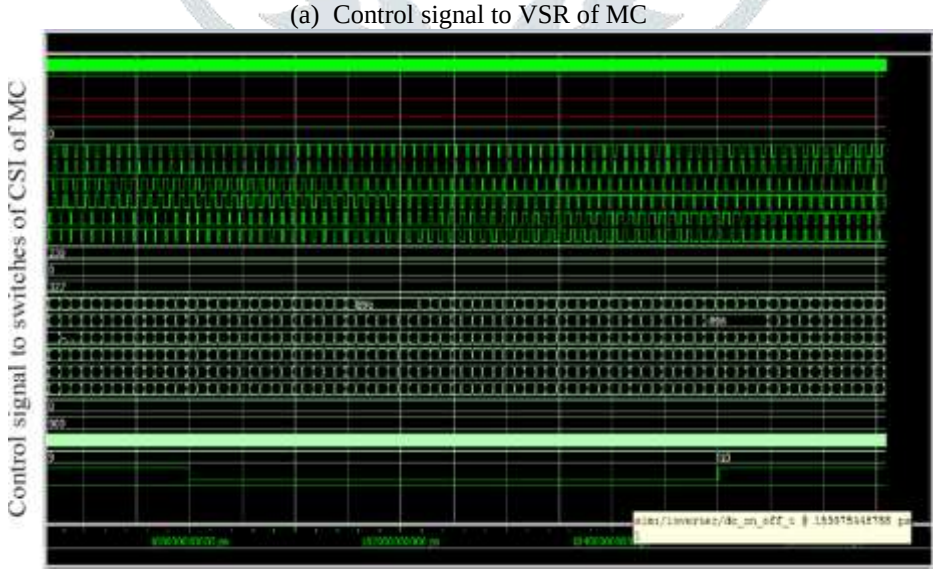

(b) Control signal to CSI of MC

(c) Control signal to dc drive based wind turbine emulator

Fig.14: SVPWM switching signals to MC and dc drive based wind turbine emulator

V. SIMULATION RESULTS AND DISCUSSION

Response during Steady-State Condition

Figure 15 shows simulation results obtained for grid connected mode for the proposed wind energy conversion system. The figure shows the waveforms for grid voltage and current, matrix converter input and output voltage and current, generator voltage and current, wind speed curve, pitch angle curve and the stator voltage and current of the proposed system. Form the simulated results of Fig.15; it is found that grid phase voltage and current are sinusoidal and properly balanced with unity power factor. The slight phase leg is due to filter. Fig.16 verifies total harmonic distortion (THD) of the grid and converters voltage and current are less than 5% which consent with permissible limits of the IEEE-519 standards.

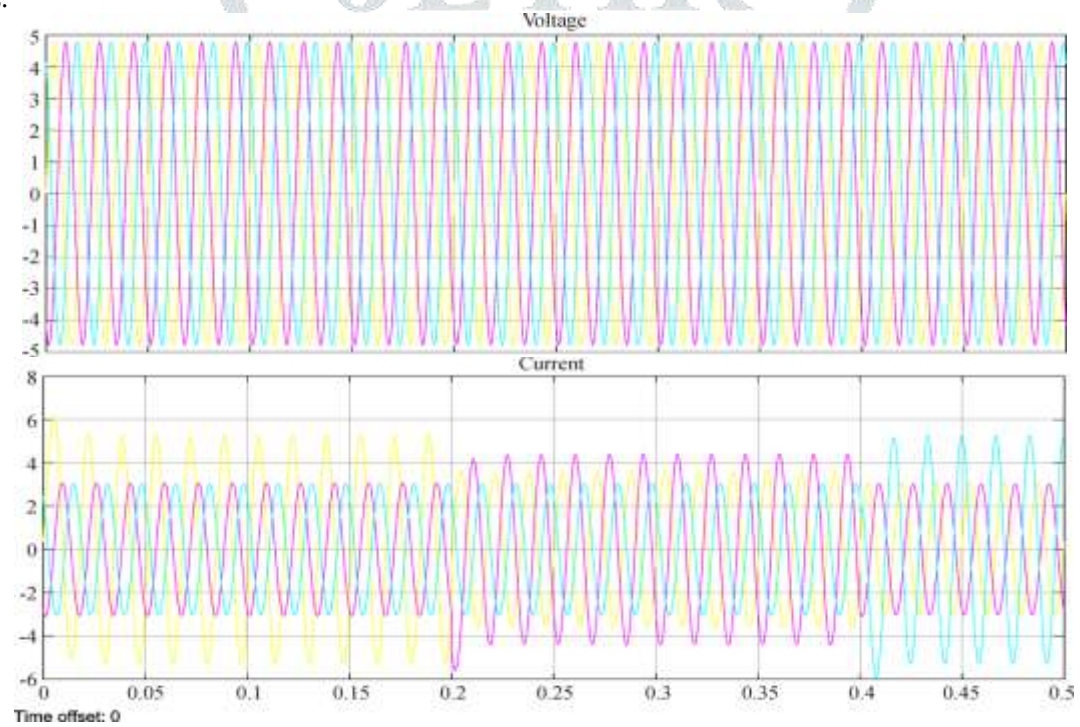

(a)

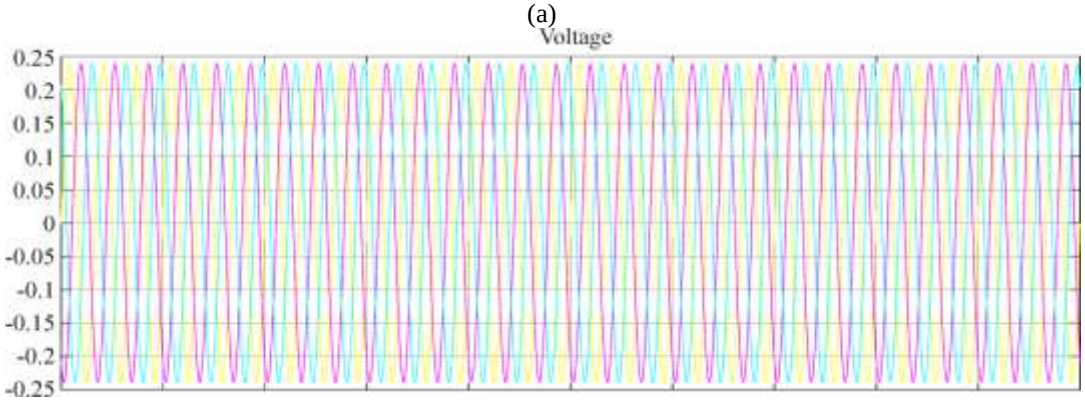

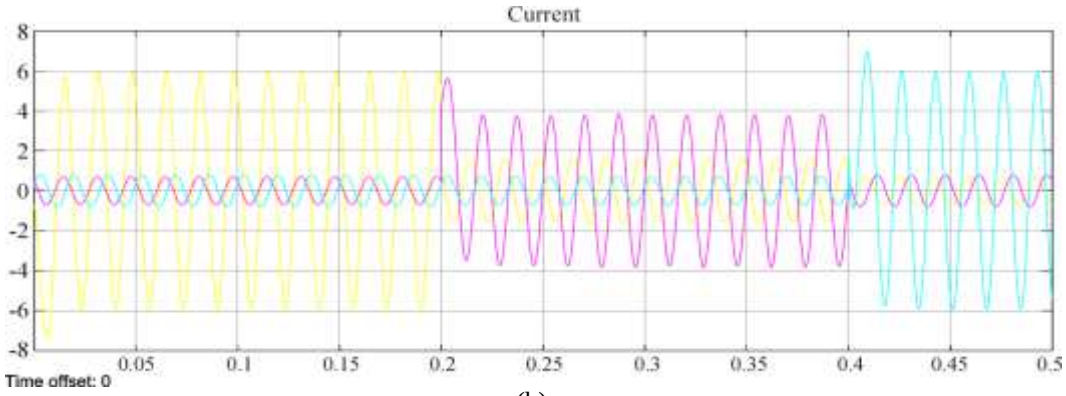
Current
Time offset: 0

(b)

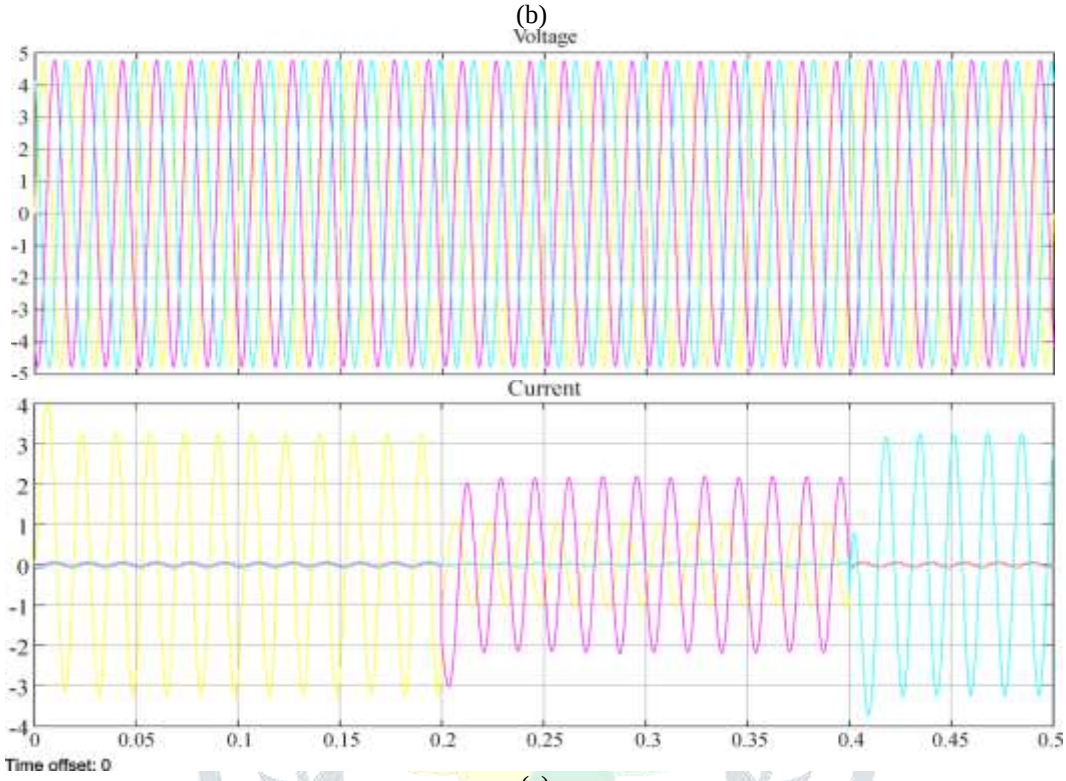
Voltage
Current
Time offset: 0

(c)

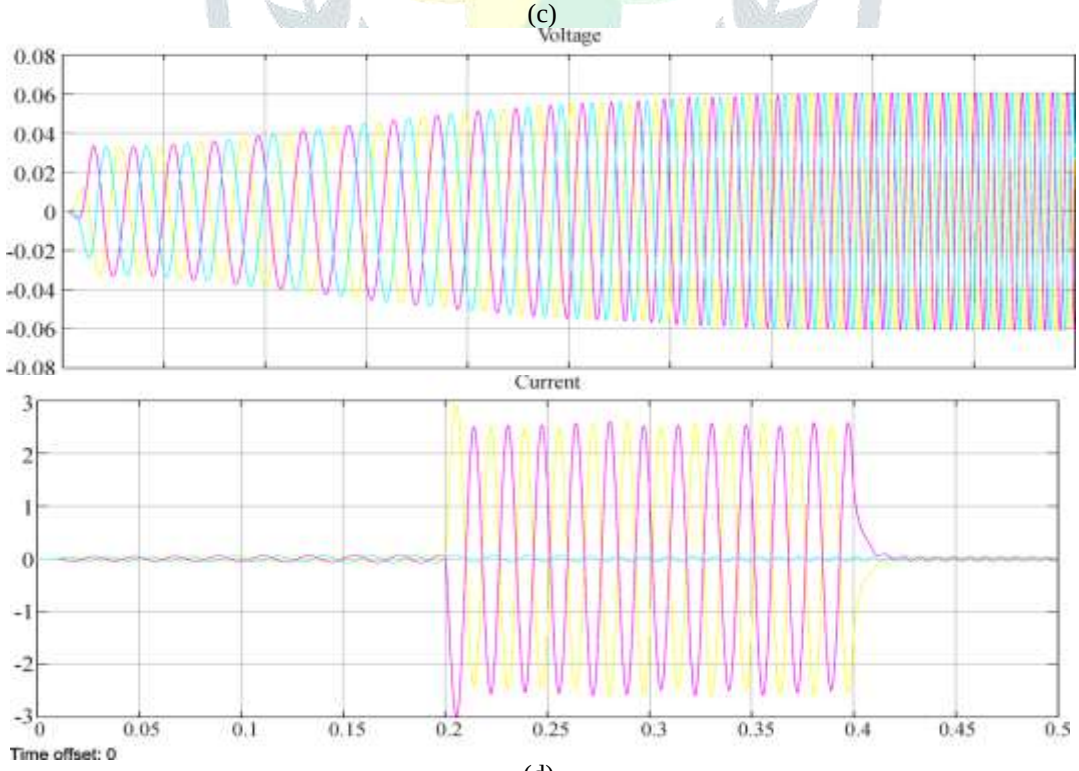
Voltage
Current
Time offset: 0

(d)

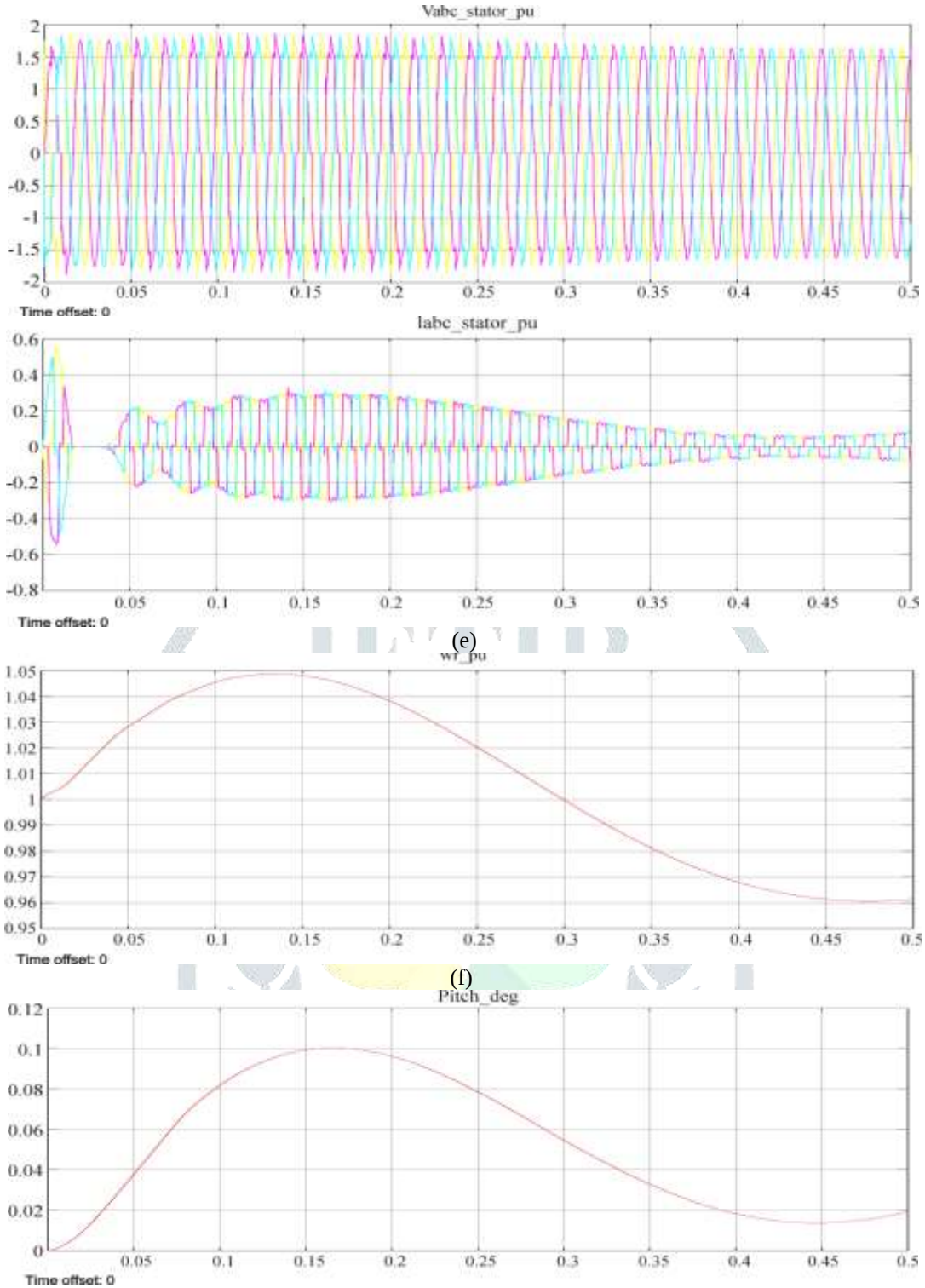

Fig. 15: Simulated responses during steady-state condition. (a) Grid voltage (pu), grid current (pu), (b) matrix converter output voltage and current, (c) matrix converter input voltage and current, (d) generator voltage and current, (e) stator voltage and current, (f) wind speed curve, (g) Pitch angle curve.

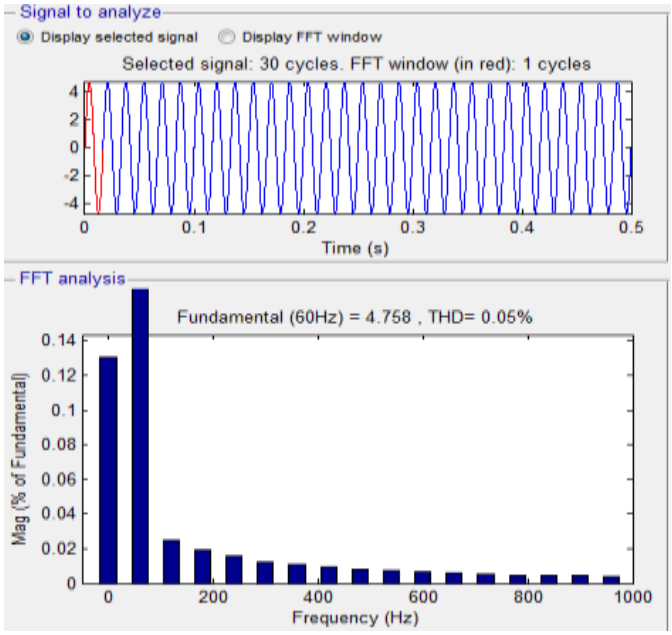

(a)

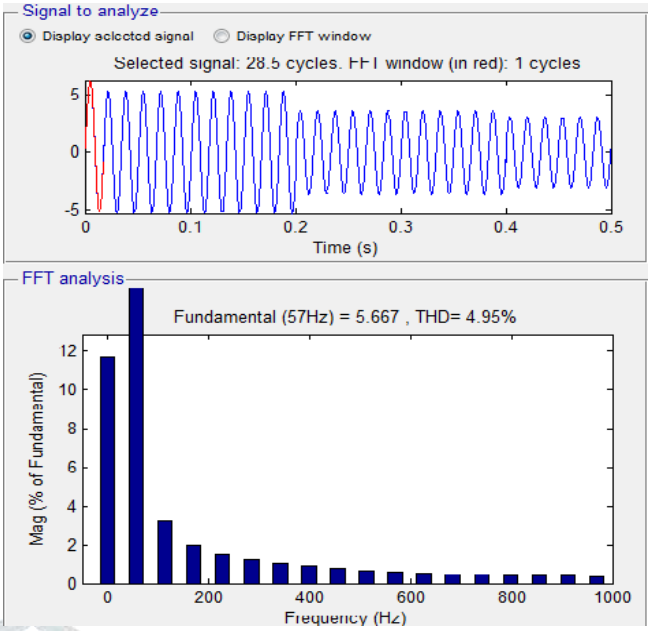

(b)

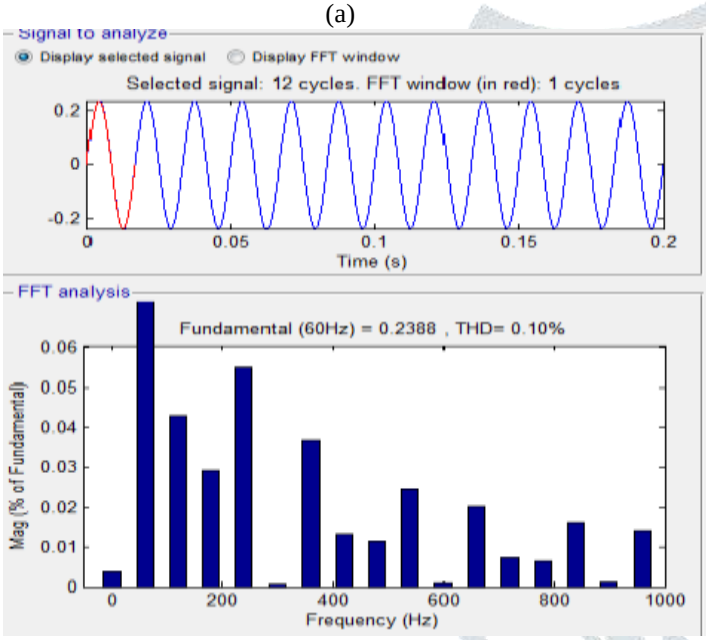

(c)

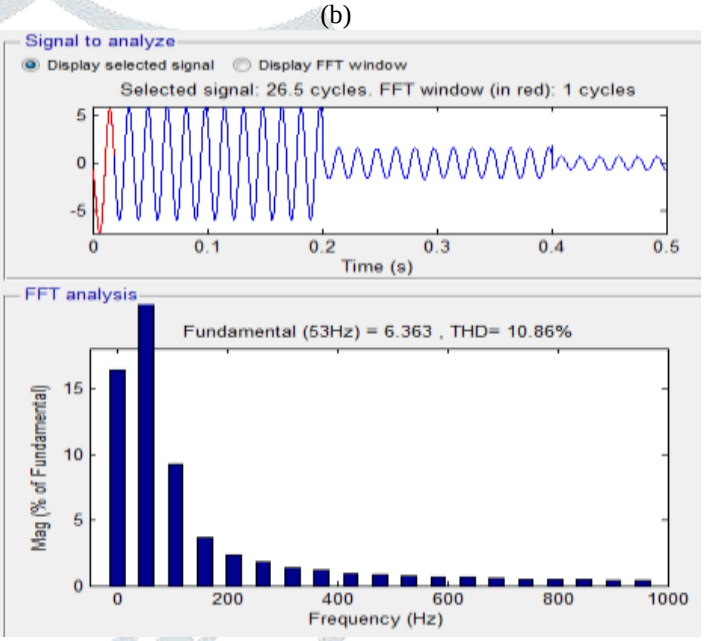

(d)

Fig. 16: FFT analysis during steady-state condition. (a) Grid voltage, (b) Grid current, (c) matrix converter voltage, (d) matrix converter current

Response during System Fault Condition

The developed wind energy conversion system has been run using MATLAB/ Simulink and Sim Power System Toolbox under different phase to ground, single phase, two phase and three phase faults, which causes dips in the system. Figure 17 show the simulated response of the proposed wind energy conversion system during fault conditions.

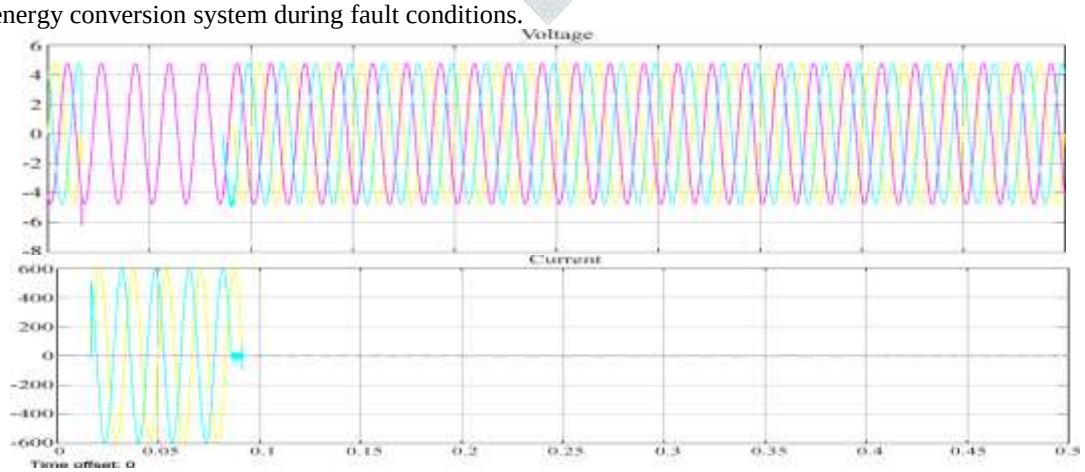

(a)

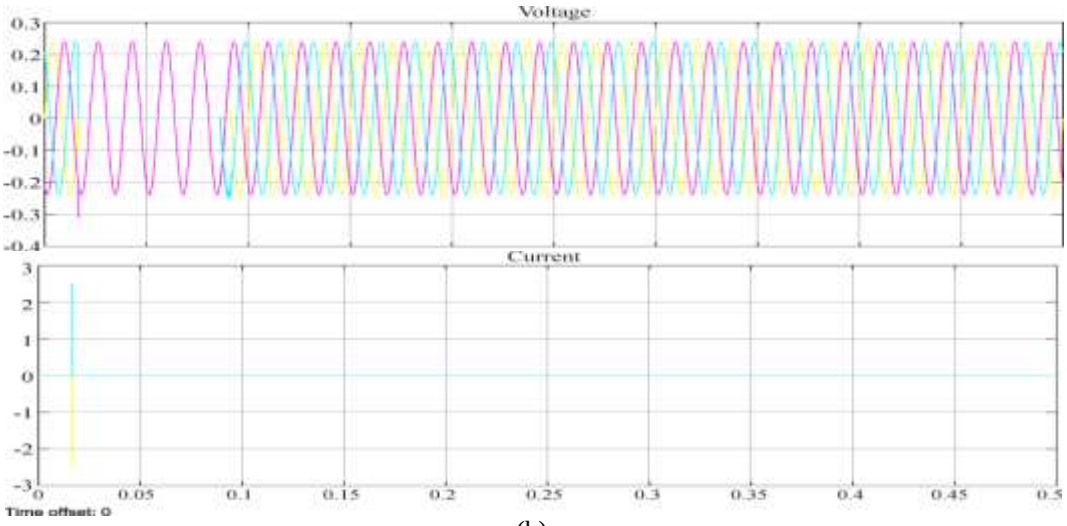

(b)

Fig. 17: Simulated responses during two phase to ground fault. (a) Grid voltage (pu), grid current (pu), (b) matrix converter voltage, matrix converter current

Converter Input and Output Response

Figure 18 shows simulation results obtained from grid connected mode for the proposed wind energy conversion system. The figure shows the converter input and output response.

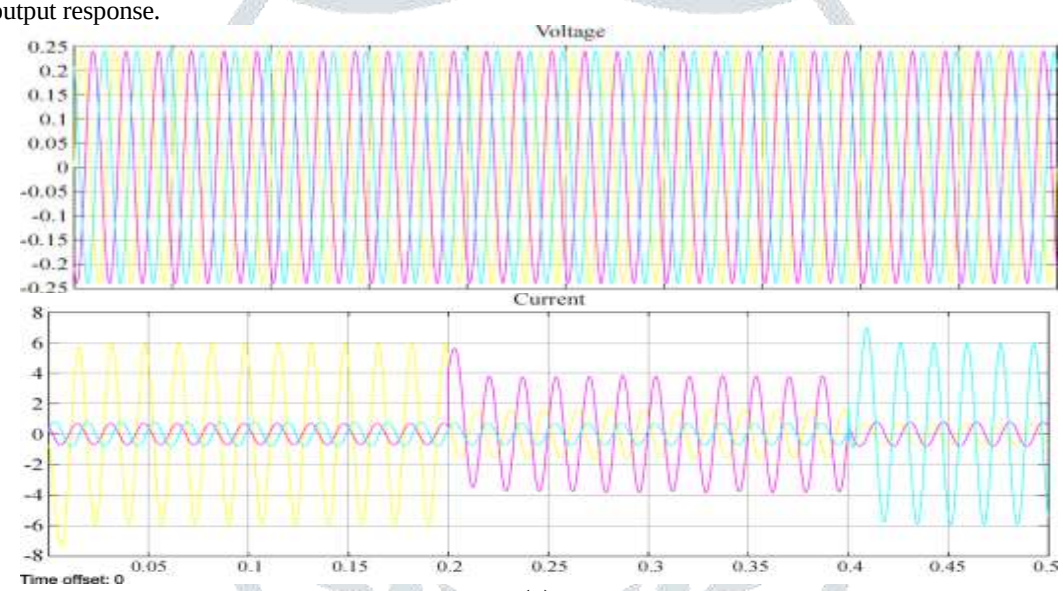

(a)

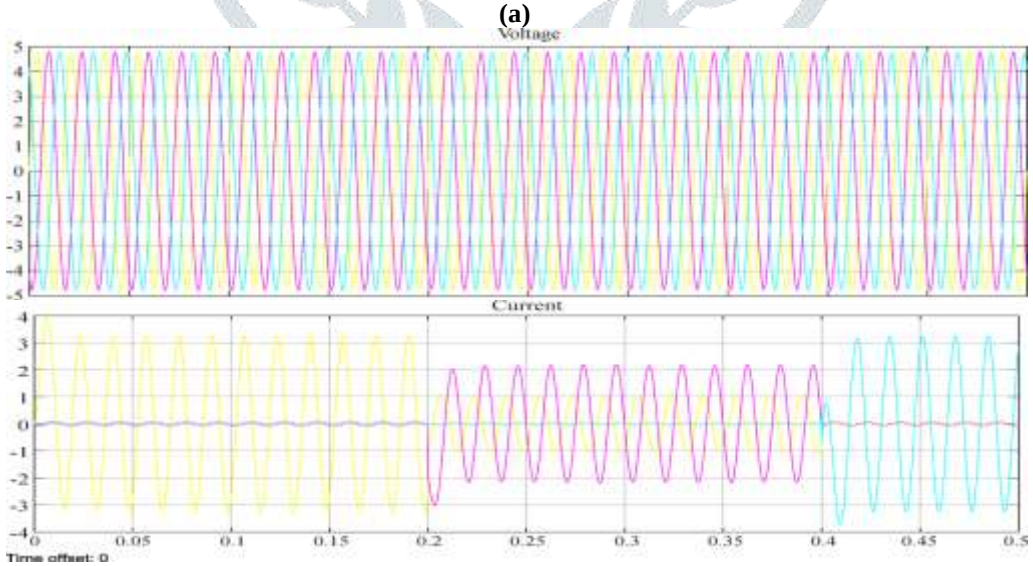

(b)

Fig. 18: Simulated responses for converter (a) MC output voltage and current, (b) MC input voltage and current

VI. EXPERIMENTAL RESULTS AND DISCUSSION

Detailed experimentation is performed on the laboratory 1.2kW prototype of matrix converter based wind energy conversion system under both isolated mode for different balanced/unbalanced load and wind/load conditions. In isolated mode, performance of the laboratory prototype of matrix converter based WECS is investigated under different resistive, non-linear inductive and dc loads at different speeds.

Response during constant resistive and non-linear inductive load

During isolated mode, wind turbine is controlled to deliver power to an external load through unidirectional indirect voltage boosted matrix

converter. Here, the objective of the developed control is to keep regulated voltage across the load. Prototype has been tested experimentally under different resistive and non-linear inductive load ranging from no load to 2.5 kW at different generator speeds.

Figures 19 and 20 illustrate various experimental waveforms of three phase load voltage, load current, harmonic spectrum for load voltage and current, fictitious dc link voltage, generator output voltage, generator output current, generator voltage and current harmonic spectrum, and generator phase voltage and current for resistive load of 1 kW and generator speed of 1200 rpm and 1600 rpm, respectively.

From experimental waveforms of Fig. 19(a,b) and Fig. 20(a,b), a good equilibrium among the load currents and voltages can be seen. Also, the load voltage and current waveforms are properly balanced. It can also be observed from Fig. 19 (a) and (b), and 20 (a) and (b) that three phase load current and voltages are well regulated sinusoidal with unity power factor operation for resistive load. Also, it can be seen that PMSG phase voltage, current, fictitious dc link voltage, MC voltage and the load voltage for resistive load are within safe limits.

From load voltage and current harmonic spectrum of Fig. 19 (c,d) and Fig. 20 (c,d), it can be seen that total harmonic distortion (THD) of load voltage and load current is 2.3% and 2.4 % respectively, which is less than 5% and it is in consent with the permissible limits of IEEE 1547, IEEE-519 and IEC 61727 standards and thus satisfies the general standards of produced power in terms of voltage and current inside 5% THD. Low THD is due to the use of space vector pulse width modulation (SVPWM) switching for the matrix converter.

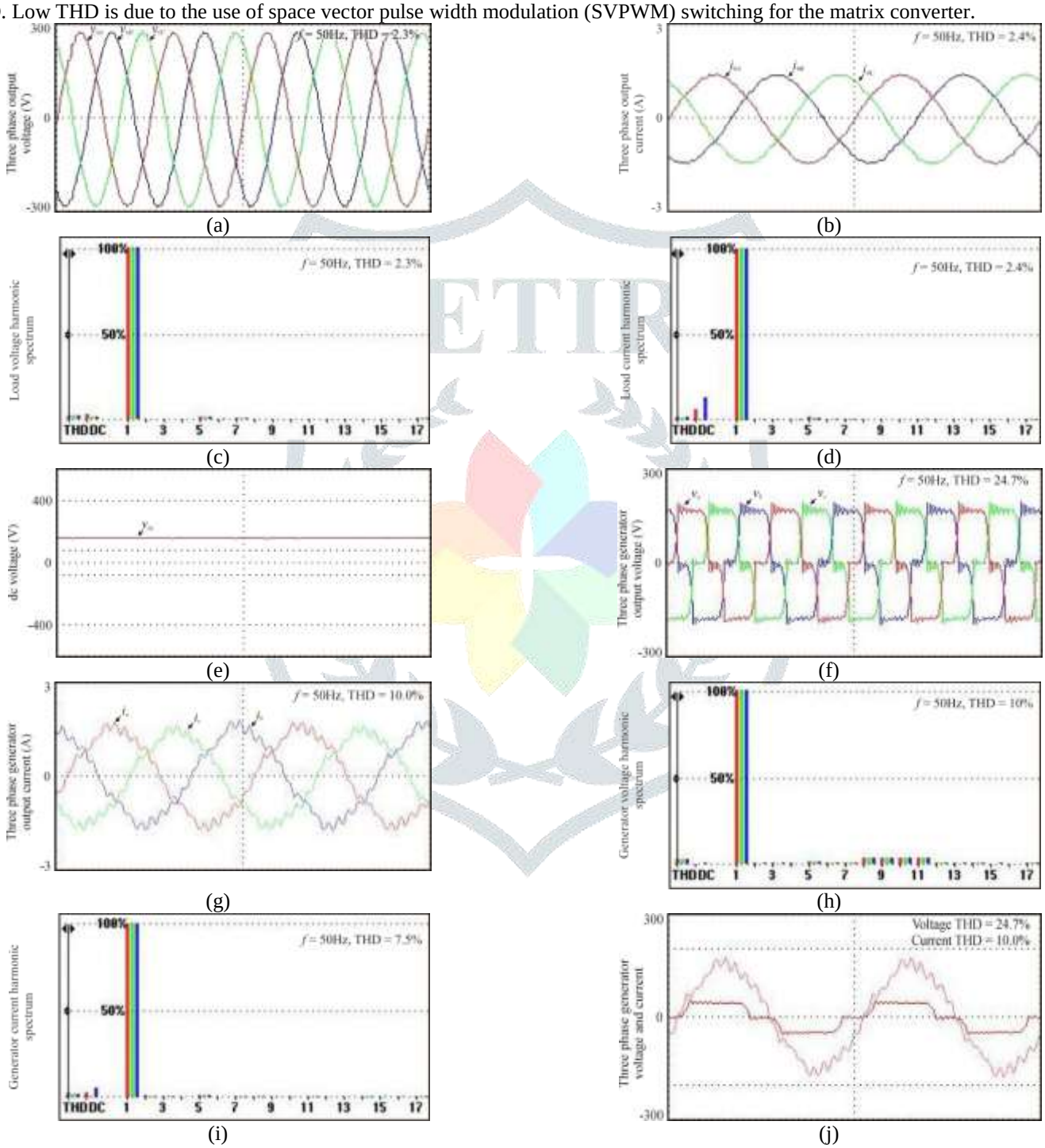

Fig. 19: Experimental waveforms during constant resistive load of 1 kW, 1200 rpm: (a) three-phase output voltage; (b) three-phase output current; (c) load voltage harmonic spectrum; (d) load current harmonic spectrum; (e) fictitious dc link voltage; (f) generator output voltage; (g) generator output current; (h) generator voltage harmonic spectrum; (i) generator current harmonic spectrum; and (j) generator phase voltage and current.

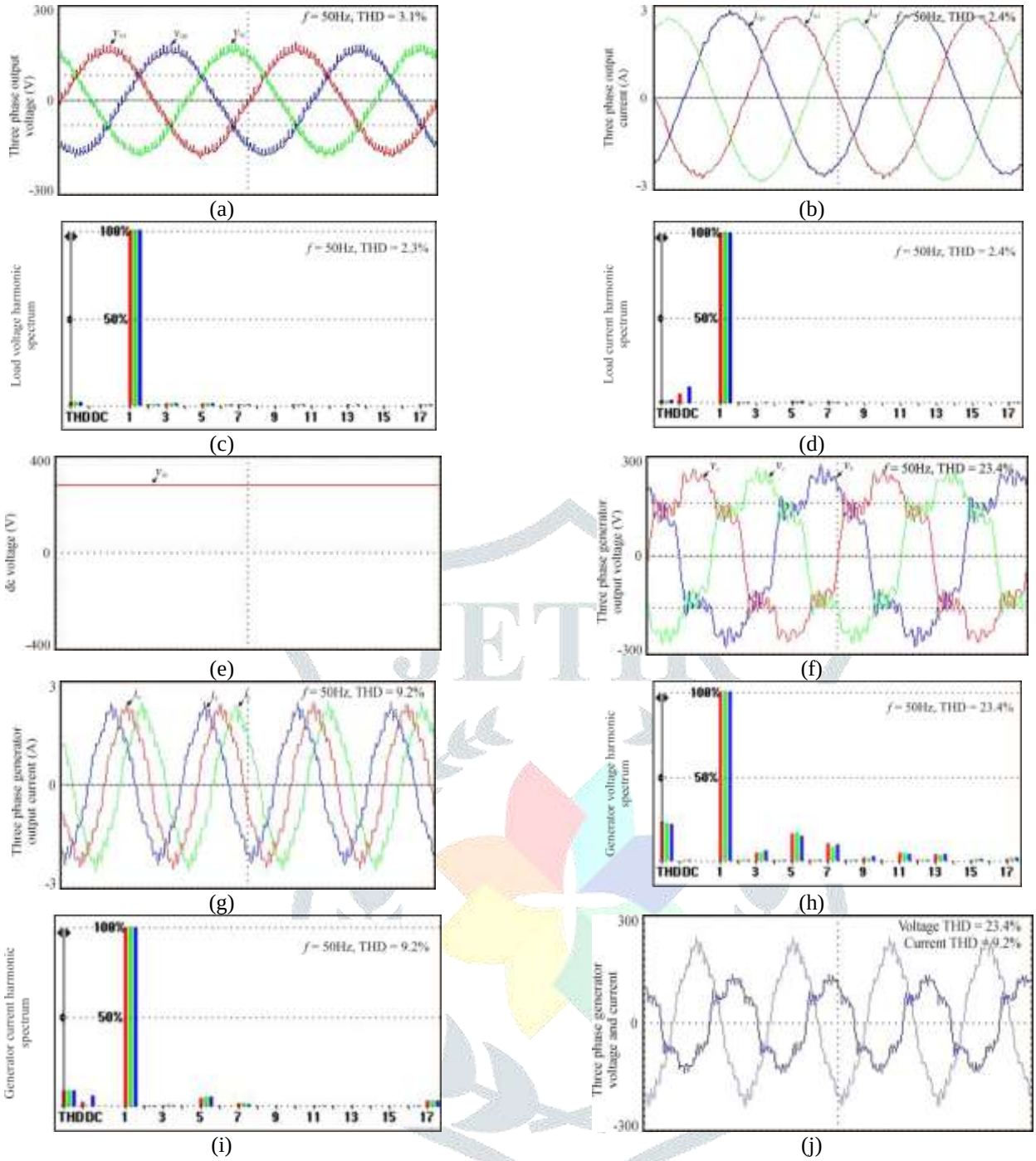

Fig. 20: Experimental waveforms during constant resistive load of 1 kW, 1600 rpm: (a) three-phase output voltage; (b) three-phase output current; (c) load voltage harmonic spectrum; (d) load current harmonic spectrum; (e) fictitious dc link voltage; (f) generator output voltage; (g) generator output current; (h) generator voltage harmonic spectrum; (i) generator current harmonic spectrum; and (j) generator phase voltage and current.

Unity power factor operation with low THD satisfies the power factor demand, and is far better as compare to power factor and THD of about 0.94% and 4.25%, respectively in case of converter topology proposed for wind power applications in [11]. This improvement in power factor results into reduction of about 13% generator conduction losses. It demonstrates the expected improvement when compared with similar works. Therefore, it is clear that the SVPWM based matrix converter interfaced WECS succeeds in regulating the load voltage and frequency within satisfied limits of 220/400 V and 50 Hz, respectively, with low-harmonic characteristics.

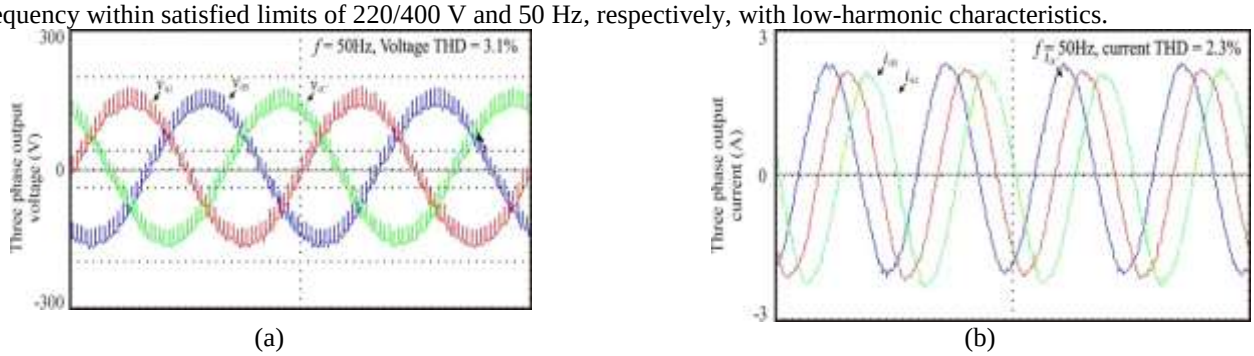

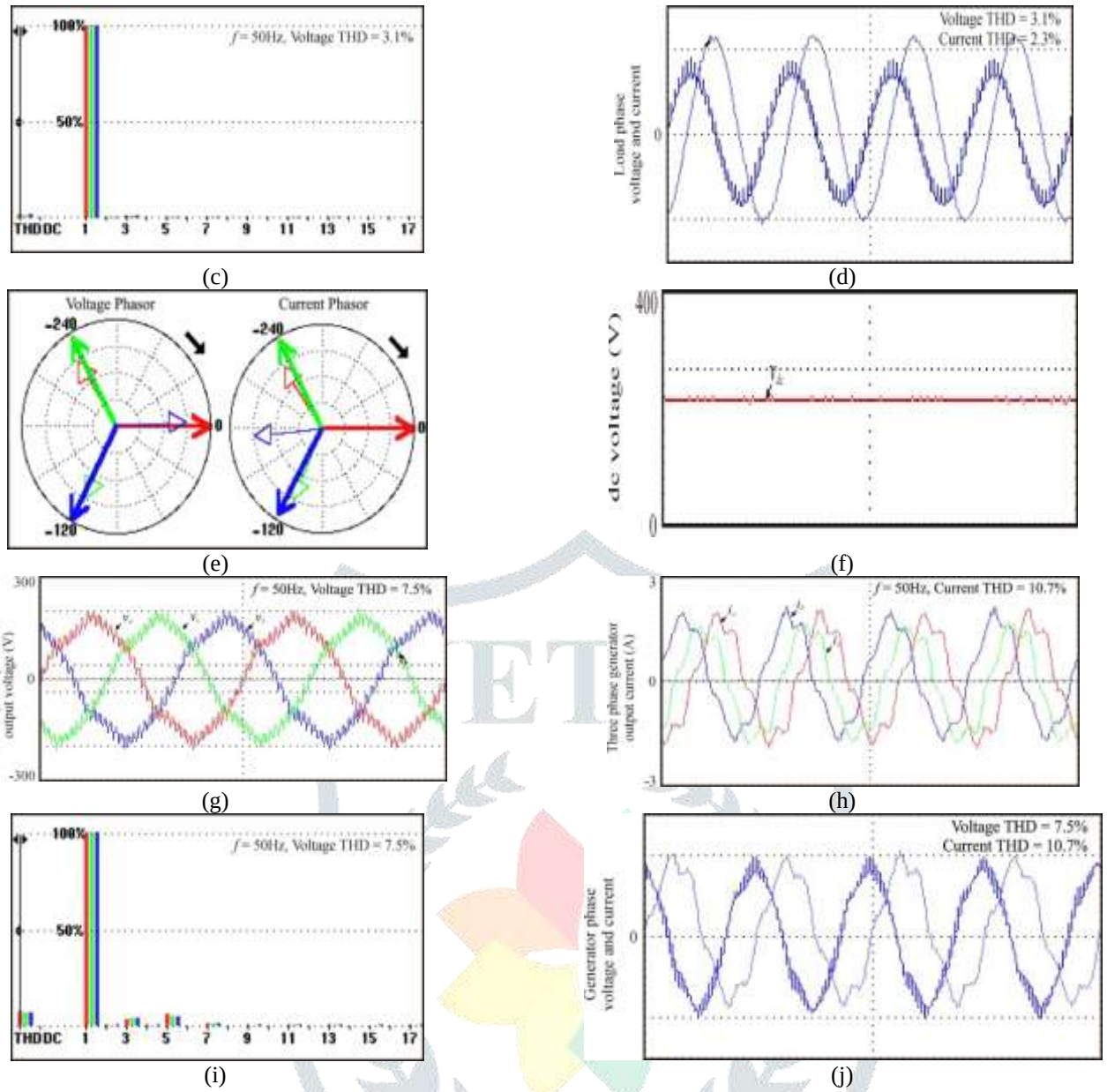

Fig. 21: Experimental waveforms during constant non-linear inductive load of 1kW, 1600 rpm: (a) load voltage; (b) load current; (c) load voltage harmonic spectrum; (d) load phase voltage & current; (e) load voltage & current phasor; (f) fictitious dc link voltage; (g) generator output voltage; (h) generator output current; (i) generator voltage harmonic spectrum; (j) generator phase voltage and current.

Figures 21 illustrate various experimental waveforms of load voltage, load current, harmonic spectrum for load voltage, load phase voltage and current, phasor diagram for load voltage and current, fictitious dc link voltage, generator output voltage, generator output current, generator voltage harmonic spectrum, generator phase voltage and current, transients in load voltage and current, and field voltage for non-linear inductive load of 1 kW and 1.5 kW with generator speed of 1600 rpm, respectively. Here, in this work, diode rectifier-inverter fed three-phase induction motor is used as a non-linear load. Almost similar findings in terms of power factor, THD, frequency is achieved in case of non-linear inductive load, except little more THD due to non-linear nature of load, but it was also quite within the limits as per standards.

Response during varying load condition

Figures 22 demonstrate the effectiveness of the proposed controls for developed laboratory prototype of WECS during various dynamic conditions. Figure 22 shows the response of instantaneous load current, fictitious dc link voltage, dc link current, MC output current, generator current, and output load voltage under varying load. The load is changed from 100% to 50% and then from 50% to 100% to simulate the transient load changing. It is observed that load voltage is well maintained despite the variation of loads. But, the load current is changing with load variation as expected.

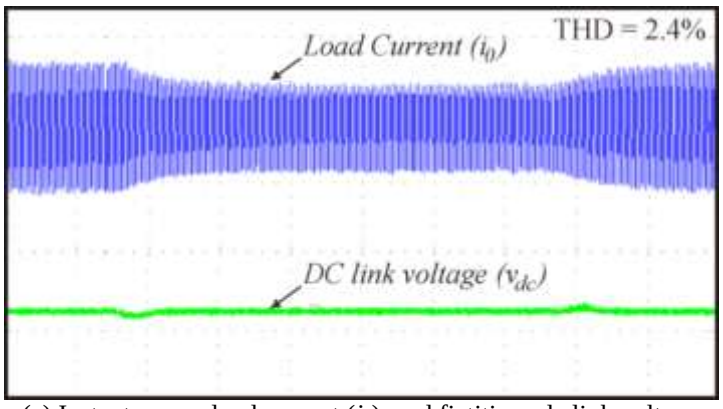

(a) Instantaneous load current (i_0), and fictitious dc link voltage (v_{dc})

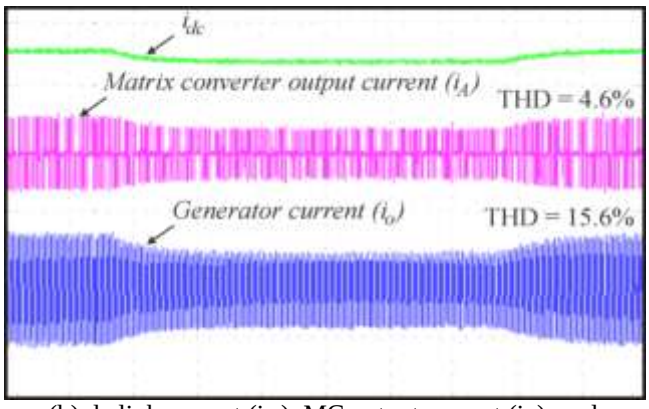

(b) dc link current (i_{dc}), MC output current (i_A), and generator current (i_0)

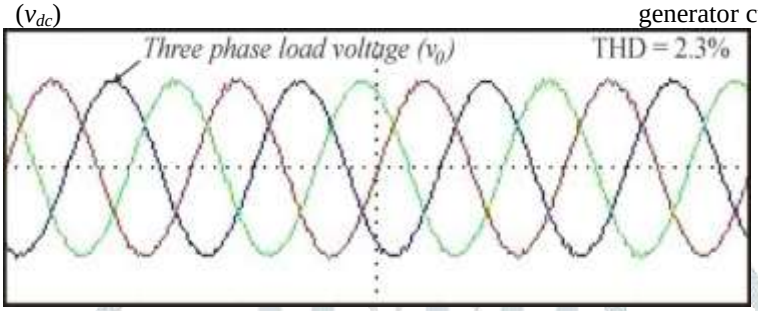

(c)

Fig. 22: Experimental waveform during varying load condition: (a) load voltage, and fictitious dc link voltage (b) dc link current, MC output current, and generator current; (c) three phase load voltages response when the load changes from 100% to 50% and then from 50% to 100%.

It is seen that the controller can regulate the load voltage and frequency quite well under varying load conditions. When the load is changed to smaller value, the load current is decreased and so closed loop control commands the necessary control action to maintain the constant voltage magnitude. On the other hand, when load is changed to larger value, load current is increased and controller keeps the load voltage constant, as expected. The experimental results indicate that the generation system is able to stabilize load voltage under varying load changing by regulating the modulation index of MC.

Dynamic response during de-blocking the control signal to matrix converter

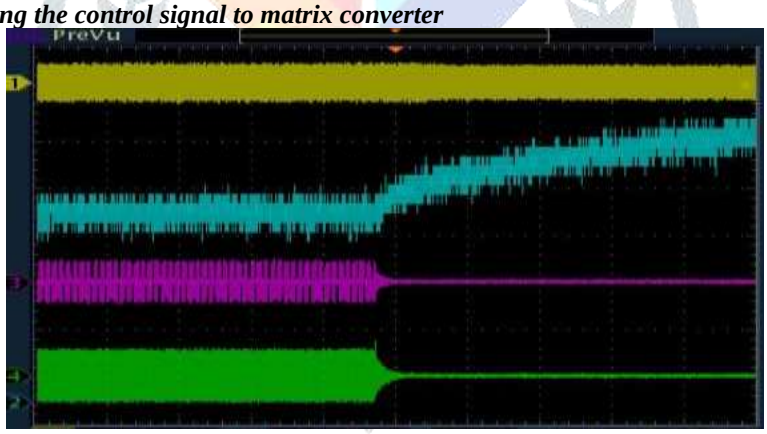

Figure 23: Experimental waveform, Ch1: generator current, Ch2: fictitious dc-link current, Ch3:MC output current, Ch4:load current respectively during sudden de-blocking of CSI pulses of matrix converter.

Laboratory prototype is also validated for exploring its fault and disturbance ride through capabilities during de-blocking the gate signals to CSI part of matrix converter. Figure 23 illustrates the experimental response of generator voltage, dc link voltage, matrix converter output current, and injected grid current during this condition. It can be seen that clamping circuit connected to the fictitious dc link clamps the dc voltage within safe limits to protect converter during such faulty abnormal conditions. Also, the response is slower, in order to keep low THD and satisfactory operation.

Dynamic response during sudden and successive step change in wind speed

To validate the maximum power point tracking capability of the proposed MC interfaced WECS is tested experimentally under sudden and successive step increase and decrease of wind speed. Experimental waveform in Figure 24 illustrates the dynamic response of generator output current, fictitious dc-link current, MC output current, and load current under sudden varying wind conditions, validating the effectiveness of tracking the MPP to yield maximum power and energy.

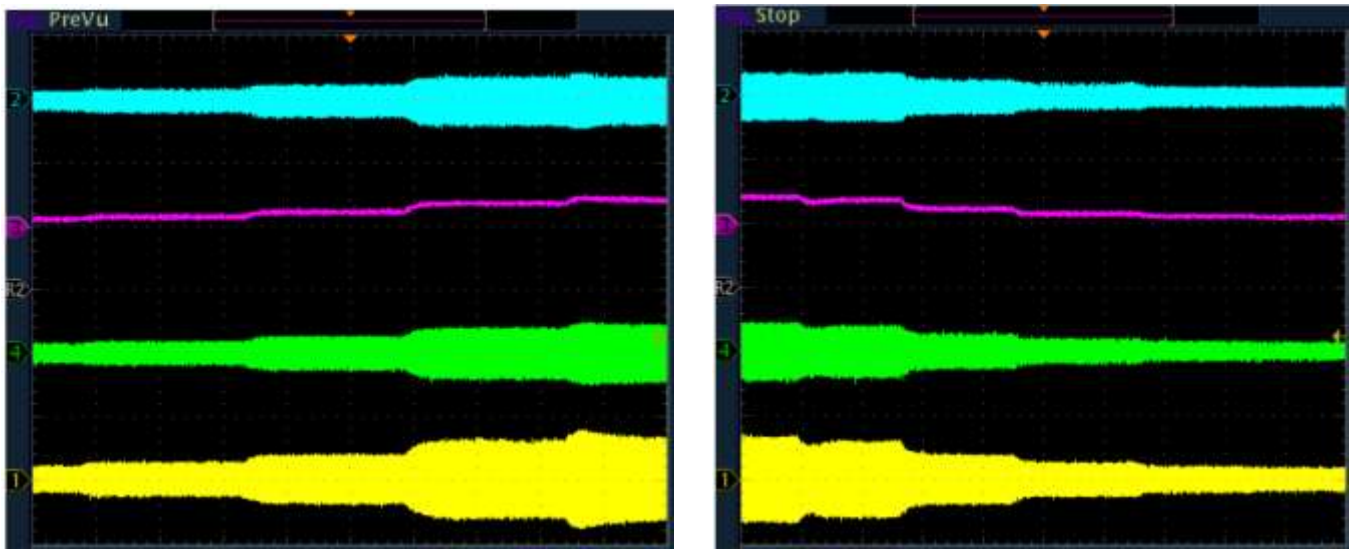

(a) Successive step rise (b) Successive step decay

Fig. 24: Experimental dynamic response of generator current (ch: 2), fictitious dc-link current (ch: 3), MC output current (ch: 4), and load current (ch: 1)during step change of wind speed.

VII. Conclusion

In this work, Performance Investigation of the Matrix Converter interfaced Wind Energy Conversion System through Simulation and Experimentation is carried out. Here, space vector modulation for indirect AC/AC converters in wind energy application is applied to have low harmonic characteristics. The SVPWM scheme is more popular than conventional technique because it gives 15% more output voltage than SPWM and prevents unnecessary switching, hence less commutation losses. Various important concluding points in this paper are as:

- It presents step-by-step and in a clear way following the ISVM switching of matrix converter to control wind energy conversion system.
- Performance for SVM switching based matrix converter fed WECS system was investigated using MATLAB/Simulink under different conditions. The response of fictitious grid voltage and the grid currents during the fault period is important to be examined in order to determine the ride-through capabilities of the developed WECS.
- Performance of the laboratory prototype of matrix converter based WECS is investigated under different constant and varying resistive, non-linear inductive and dc loads at different speeds.
- A good equilibrium among the load currents and voltages can be seen from the experimental results. Also, the load voltage and current waveforms are properly balanced and well regulated sinusoidal with unity power factor operation for resistive load.
- Total harmonic distortion (THD) of load voltage and load current is 2.3% and 2.4 % respectively, which is less than 5% which consent with the permissible limits of IEEE standard 1547, IEEE-519 and IEC 61727 and thus satisfies the general standards of produced power in terms of voltage and current inside 5%. Low THD is due to the use of space vector pulse width modulation (SVPWM) switching for the matrix converter.
- During varying load condition, it is observed that load voltage is well maintained despite the variation of loads. But, the load current is changing with load variation as expected.

References

[1] Polinder, H., Bang, D., Van, R., McDonald, A. S. and Mueller, M.A. 2007. 10 MW Wind Turbine Direct-Drive Generator Design with Pitch or Active Speed Stall Control. IEEE International on Electric Machines & Drives, 2:1390-1395.

[2] Chinchilla, M., Arnaltes, S. and Burgos 2006. Control of permanent-magnet generators applied to variable-speed wind-energy systems connected to the grid. IEEE Transactions on Energy Conversion, 21(1):130-135.

[3] Grabic, S., Celanovic, N. and Katic, V.A. 2008. Permanent magnet synchronous generator cascade for wind turbine application. IEEE Transaction on Power Electronics, 23(3):1136–1142.

[4] Pahlevaninezhad, M., Eren, S., Bakhshai, A. and Jain, P. 2009. A Model Reference Adaptive Controller for a Wind Energy Conversion System Based on a Permanent Magnet Synchronous Generator Fed by a Matrix Converter. In proceedings of 35th annual conference of the IEEE Industrial Electronics Society, 65-70.

[5]Yang, A.G. and Li, B.H. 2010. Application of a Matrix Converter for PMSG Wind Turbine Generation System. In proceedings of 2nd IEEE International Symposium on Power Electronics for Distributed Generation Systems, 619-623.

[6] Wang, H., Nayar, C., Su, J. and Ding, M. 2011. Control and Interfacing of a Grid-Connected Small-Scale Wind Turbine Generator. IEEE Transactions on Energy Conversion, 26(2):428-434.

[7] Nishida, K., Ahmed, T. and Nakaoka, M. 2011.A Cost-Effective High-Efficiency Power Conditioner with Simple MPPT Control Algorithm for Wind-Power Grid Integration. IEEE Transactions on Industry Applications, 47(2):893-900.

[8] Yun, D., Han, B. and Choi, N. 2009. Hardware simulator for PMSG wind power system with matrix converter. In proceeding of IEEE 31st International Telecommunications Energy Conference, 18-22.

[9] Chen, J., Chen, J. and Gong, C. 2013. On Optimizing the Transient Load of Variable-Speed Wind Energy Conversion System During the MPP Tracking Process. IEEE Transactions on Industrial Electronics, (99):1-10.

[10] Yang, A.G. and Li, B.H. 2010. Application of a Matrix Converter for PMSG Wind Turbine Generation System. In proceedings of 2nd IEEE International Symposium on Power Electronics for Distributed Generation Systems, 619-623.

[11] Oliveira, D.S., Reis, J.M., Silva, C.E.A., Barreto, L.H., Fernando L. M. and Bruno L.S. 2010. A Three-Phase High-Frequency Semicontrolled Rectifier for PM WECS. IEEE Transactions on Power Electronics, 25(3):677-685.